Bioorganic & Medicinal Chemistry 18 (2010) 8463–8477

Contents lists available at ScienceDirect

Bioorganic & Medicinal Chemistry

journal homepage: www.elsevier.com/locate/bmc

Synthesis, binding studies and molecular modeling of novel cannabinoid receptor ligands

Noha A. Osman [a], Amr H. Mahmoud [b], Marco Allarà [c], Raimund Niess [a], Khaled A. Abouzid [b], Vincenzo Di Marzo [c], Ashraf H. Abadi [a,*]

[a] Department of Pharmaceutical Chemistry, Faculty of Pharmacy and Biotechnology, German University in Cairo, Al Tagamoa Al Khames, New Cairo City 11835, Egypt
[b] Department of Pharmaceutical Chemistry, Faculty of Pharmacy, Ain Shams University, Cairo 11566, Egypt
[c] Endocannabinoid Research Group, Institute of Biomolecular Chemistry, Consiglio Nazionale delle Ricerche, Via Campi Flegrei 34, 80078 Pozzuoli, Napoli, Italy

ARTICLE INFO

Article history:
Received 30 August 2010
Revised 16 October 2010
Accepted 19 October 2010
Available online 27 October 2010

Keywords:
Endocannabinoids
CB2 selectivity
Anandamide derivatives
Homology modeling

ABSTRACT

In the present work, we report upon the design, synthesis and biological evaluation of new anandamide derivatives obtained by modifications of the fatty acyl chain and/or of the ethanolamide 'tail'. The compounds are of the general formula: 6-(substituted-phenyl)/naphthyl-4-oxohex-5-enoic acid *N*-substituted amide and 7-naphthyl-5-oxohept-6-enoicacid *N*-substituted amide. The novel compounds had been evaluated for their binding affinity to CB1/CB2 cannabinoid receptors, binding studies showed that some of the newly developed compounds have measurable affinity and selectivity for the CB2 receptor. Compounds **XI** and **XVIII** showed the highest binding affinity for CB2 receptor. None of the compounds exhibited inhibitory activity towards anandamide hydrolysis, thus arguing in favor of their enzymatic stability. The structure–activity relationship has been extensively studied through a tailor-made homological model using constrained docking in addition to pharmacophore analysis, both feature and field based.

1. Introduction

Marijuana or hashish, derived from the Indian hemp *Cannabis sativa* have been used for medical purposes in Chinese and Egyptian sources as early as 2700 BC. Apart from its medical use, marijuana gained great popularity as a recreational drug due to the presence of the psychotropic component '(−)-trans-Δ^9-tetrahydrocannabinol' (THC), which has the ability to cause euphoria and elation.[1] It was the identification Δ^9-THC as the major psychoactive ingredient in cannabis, as well as its chemical synthesis that led to the discovery of the cannabinoid receptors: CB1 and CB2.[2] The former is highly expressed in brain and was cloned in 1990, while the latter is expressed predominantly in the periphery and appears to be mainly associated with the immune cells and spleen.[3–5] The existence of such specific receptors that recognize phytocannabinoids stimulated the search for endogenous cannabinoid receptor ligands, the 'endocannabinoids'. By 1992, the first endocannabinoid, arachidonoyl ethanolamide (AEA or anandamide, Fig. 1), was isolated from porcine brain, and found to mimic many of the actions of THC.[6] Three years later, a second endocannabinoid, 2-arachidonoyl glycerol (2-AG), was discovered.[7,8] Both compounds are ultimately derivatives of arachidonic acid, and are biosynthesised 'on demand' from membrane phospholipids. The finding of endocannabinoids led to the discovery of three additional proteins, fatty acid amide hydrolase (FAAH), monoacylglycerol lipase (MAGL) and the putative anandamide transporter (AT), which are involved in their metabolism. Endocannabinoids signaling is terminated by a two-step process: cellular uptake, facilitated by AT, followed by enzymatic degradation by FAAH, or MAGL in case of 2-AG.[9–11] Hence, the CB1 and CB2 cannabinoid receptors, their endogenous ligands (endocannabinoids), and enzymes, proteins, and transporters involved in endocannabinoid formation and inactivation, collectively comprise the endocannabinoid system. The components of this system represent excellent targets for development of therapeutically useful drugs for a range of conditions including pain, inflammation, immunosuppression, loss of appetite and many others.[12]

The focus of this work was to design, synthesize and pharmacologically evaluate new anandamide (AEA) derivatives, obtained by modifications of the fatty acyl chain and/or of the ethanolamide 'tail'. The synthesis of novel compounds with the general formula: 6-(substituted-phenyl)-4-oxohex-5-enoicacid *N*-substituted amide and 7-naphthyl-5-oxohept-6-enoicacid *N*-substituted amide is reported in the present work (Fig. 1). All newly synthesized compounds were evaluated for their binding affinity to CB1/CB2 cannabinoid receptors. The SAR was studied extensively using

* Corresponding author. Tel.: +20 2 27590716; fax: +20 2 27581041.
E-mail addresses: ashraf.abadi@guc.edu.eg (A.H. Abadi), ahabadi@yahoo.com (A.H. Abadi).

0968-0896/$ - see front matter © 2010 Elsevier Ltd. All rights reserved.
doi:10.1016/j.bmc.2010.10.050

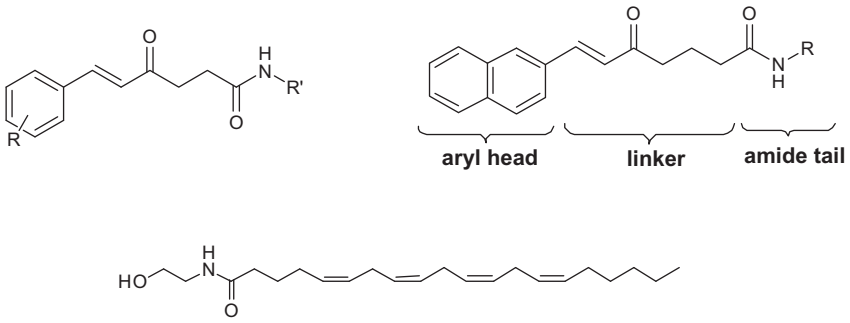

Figure 1. Chemical structure of anandamide and the general skeletons of the synthesized compounds.

tailor-made homological model, constrain docking based on site-directed mutagenesis data and pharmacophore analysis (both field and feature based).

2. Results and discussion

2.1. Chemistry

The synthesis of (*E*)-6/7-(substituted-phenyl/naphthyl)-4/5-oxohex-5/hept-6-enoic acids (**I**–**V**) (illustrated in Schemes 1 and 2) was adopted according to the general procedure previously reported in the literature. This involved condensation of the appropriate aldehyde with levulinic acid or 4-acetyl butyric acid using catalytic amounts of piperidine and acetic acid to give the respective arylidine keto acid derivatives. Three of the intermediates are reported compounds (**I**, **II** and **V**) while two of them are novel ones (**III** and **IV**).[13] When 4-acetyl butyric acid was reacted with 2-naphthaldehyde (to give compound **IV**) instead of levulinic acid (to give compound **III**), a multiplet appeared upfield at $\delta \approx 2.05$–2.10 ppm characteristic of the extra $-CH_2$ group added. Moreover, separation of the *E*-isomer is evident by the high *J* value of the olefinic protons, calculated to be $\geqslant 15$ Hz, which is typical for *E*-isomers rather than the *Z* ones. Infrared (IR) spectroscopy showed characteristic broad bands at the range of about 3300–2400 cm^{-1} for the –OH stretching of the carboxylic acid, bands at about 1690 cm^{-1} for the carboxylic –C=O stretching and bands at about 1675 cm^{-1} for the ketonic –C=O stretching. The ketonic –C=O stretching shows relatively lower values than the carboxylic acid –C=O due to the presence of an α, β double bond next to the ketonic –C=O.

The general synthesis of 6-(substituted-phenyl)-4-oxohex-5-enoic acid *N*-substituted amide and 6/7-naphthyl-4/5-oxohex-5-/hept-6-enoic acid *N*-substituted amide is described in Schemes 3 and 4, respectively. Synthesis of compounds with biphenyl aryl heads is illustrated in Schemes 5 and 6. Compounds containing secondary amides showed IR bands at about 3280 cm^{-1} of the –NH stretching, and in addition to this, –C=O stretching of the amide derivatives showed bands at relatively lower values (about 1650 cm^{-1}) than the typical carbonyl stretching at about 1700 cm^{-1}. Compounds **XIV** and **XX** showed an additional –C=O stretching band of the ester at relatively higher values (about 1738 cm^{-1}) than the typical carbonyl stretching at about 1700 cm^{-1}.

2.2. Biology and molecular modeling

All novel compounds were evaluated for their in vitro ability to bind to human recombinant CB1 and CB2 receptors and their IC_{50} and K_i values calculated. Results are shown in Table 1. The binding assay results showed that 5 out of 20 newly synthesized compounds (**XI**, **XIV**, **XVII**, **XIX** and **XXIII**) were able to bind selectively to CB2 receptor with measurable IC_{50} and K_i values in the low micromolar range and with selectivity index from 4 to 10.

To explain the SAR profile of these ligands, we developed an homology model to find the bioactive conformer of a selective CB2 agonist (GW405833)[14] (Fig. 2) and the pharmacophoric features of this ligand, and the relation between them in the space. This homology model was used for three purposes: (1) Alignment of the synthesized ligands to the bioactive conformer of the selective CB2 ligand (GW405833) using Field alignment method[15] while applying constraints on the essential field points required for activity; (2) docking with pharmacophoric restraint based on the idea that good activity should be linked with good pharmacophore constraints together with good interactions in the binding site and absence of steric clash or high torsional strain; (3) MIF (Molecular interaction field) analysis of the binding site.

To develop the CB2 homology model, the strategy of De Graff and Rognan[16] was adopted with some modifications. In short, the GPCR modeling workflow used in this study followed seven steps:

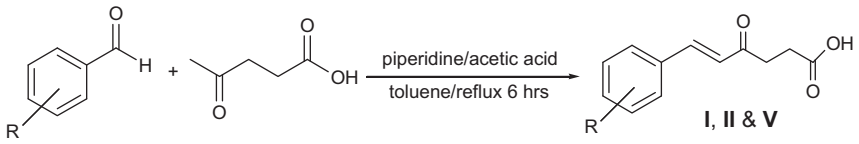

Compound	R
I	3, 4-dimethoxy
II	4-methoxy
V	4-Ph

Scheme 1.

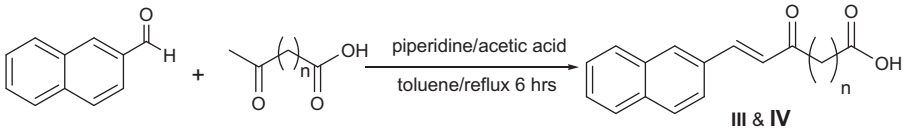

Compound	n
III	2
IV	3

Scheme 2.

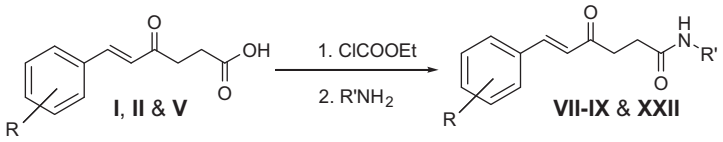

Compound	R	R'
VII	3,4 – dimethoxy	-piperidin-1-yl
VIII	3,4 – dimethoxy	$-CH_2-CH_2-OH$
IX	4-methoxy	-4-hydroxyphenyl
XXII	4-Ph	$-CH_2-CH_2-OH$

Scheme 3.

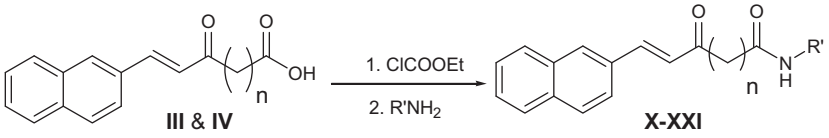

Compound	n	R'
X	2	-piperidin-1-yl
XI	2	$-CH_2-CH_2-OH$
XII	2	-4-hydroxyphenyl
XIII	2	-cyclopropyl
XIV	2	$-CH_2-COOC_2H_5$
XV	2	$-(CH_2-CH_2-OH)_2$
XVI	2	$-CH(CH_3)-CH_2-OH$
XVII	3	-piperidin-1-yl
XVIII	3	$-CH_2-CH_2-OH$
XIX	3	-cyclopropyl
XX	3	$-CH_2-COOC_2H_5$
XXI	3	$-CH(CH_3)-CH_2-OH$

Scheme 4.

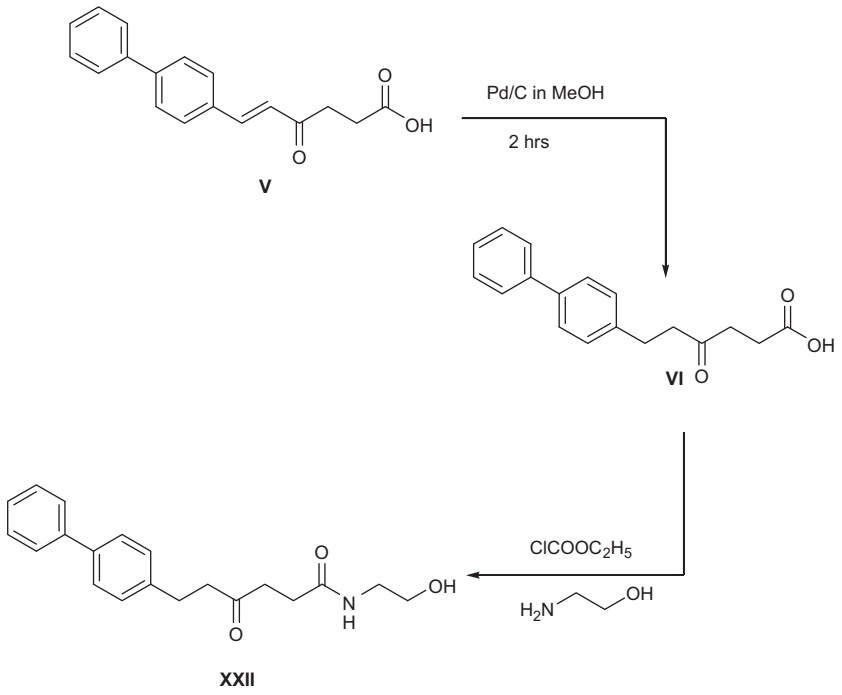

Scheme 5.

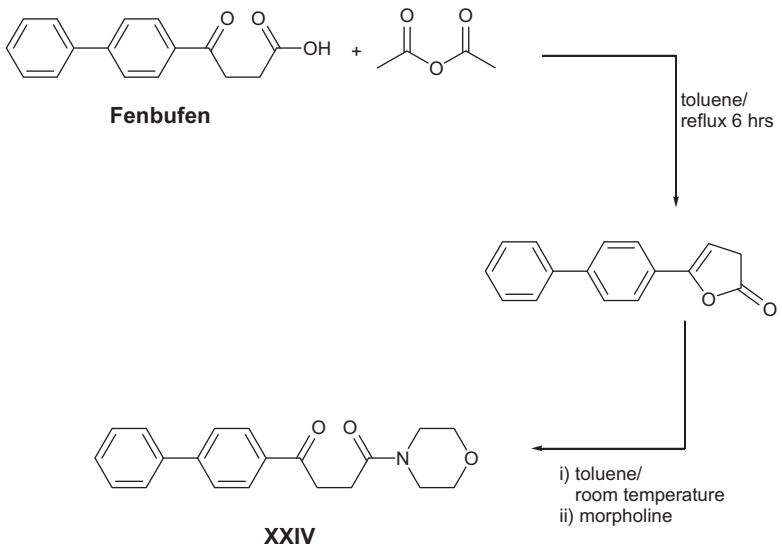

Scheme 6.

(1) Construction of the initial receptor model, consisting of the seven trans membrane (TM) helices, after identification of the TM helices (template-independent de novo modeling), amino acid sequence alignment between target and template receptors and by rotation/de novo modeling of certain TM helices with putative alternative helical kinks; (2) construction of a preliminary TM-ligand complex; (3) energy minimization of the TM-ligand complex; (4) molecular dynamics simulation refinement of the receptor–ligand complex; (5) modeling the loops connecting the TM helices; (6) selection and refinement of the full receptor–ligand complex; (7) validation of the full receptor–ligand complex was done by docking of the newly synthesized ligands. Previous studies developed CB2 homology model using Bovine rhodopsin crystal structure,[17,18] as well as the CB2 homological modeling in the inactive state using β2-adrenergic receptor as a template.[19] In this study, we built up a model to represent the active state using β2-adrenergic receptor as a template. It is known that CB2 receptors share more structural features with β2-adrenergic receptor rather than rhodopsin, for instance both CB2 and β2-adrenergic receptors may have small non covalently bound ligands, and both receptors share the Cys-X-X-X-Ar motif that is conserved in extracellular loop 2 (EC2) among GPCRs that bind biogenic amines and peptides[20,21] (Fig. 4). The T4-lysozyme inserted into the β_2 receptor between Gln231 and Ser262 to assist crystallization was removed. As the T4-lysozyme replaced ICL3, which is distant from the binding site, ICL3 was not modeled in the receptors (Supplementary data, Figs. A-1 and A-2). The CB2 and β2 sequences were aligned based on existing information on conserved residues within class-A G protein-coupled receptors,

Table 1
Results of radioligand binding assays of the synthesised compounds

Compd	Structure	Max tested on CB1 (% displacement) (μM)	IC_{50} on CB1 (μM)	K_i on CB1 (μM)	Max tested on CB2 (% displacement) (μM)	IC_{50} on CB2 (μM)	K_i on CB2 (μM)	Selectivity index (K_i CB1/K_i CB2)
III	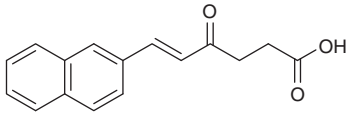	10 (11.84%)	>10	>10	10 (13.72%)	>10	>10	–
IV	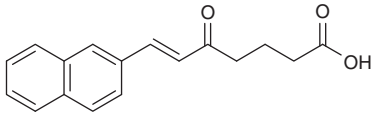	10 (21.49%)	>10	>10	10 (23.40%)	>10	>10	–
VII	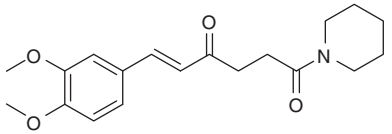	10 (<50%)	>10	>10	10 (<50%)	>10	>10	–
VIII	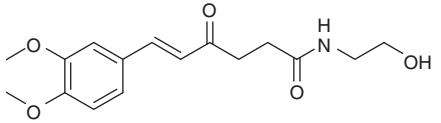	10 (<50%)	>10	>10	10 (<50%)	>10	>10	–
IX	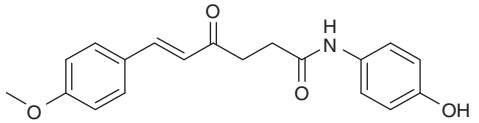	10 (<50%)	>10	>10	10 (<50%)	>10	>10	–
X	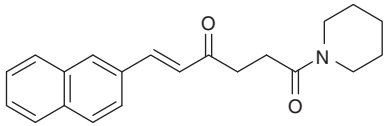	10 (<50%)	>10	>10	10 (<50%)	>10	>10	–
XI	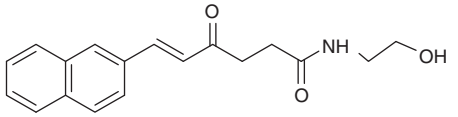	10 (0.00%)	>10	>10	10 (56.52%)	1.00	1.03	>4.41
XII	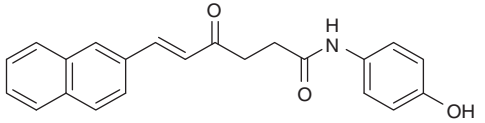	10 (<50%)	>10	>10	10 (<50%)	>10	>10	–
XIII	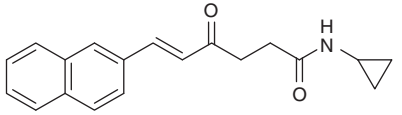	10 (3.25%)	>10	>10	10 (35.64%)	>10	>10	–
XIV	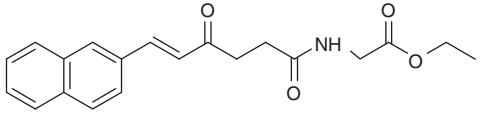	10 (5.73%)	>10	>10	10 (54.63%)	9.82	2.50	>4.00

(*continued on next page*)

Table 1 (*continued*)

Compd	Structure	Max tested on CB1 (% displacement) (μM)	IC_{50} on CB1 (μM)	K_i on CB1 (μM)	Max tested on CB2 (% displacement) (μM)	IC_{50} on CB2 (μM)	K_i on CB2 (μM)	Selectivity index (K_i CB1/K_i CB2)
XV	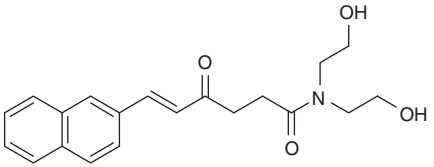	10 (1.81%)	>10	>10	10 (27.32%)	>10	>10	–
XVI	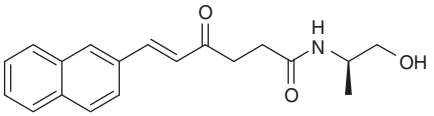	10 (+2.48%)	>10	>10	10 (38.28%)	>10	>10	–
XVII	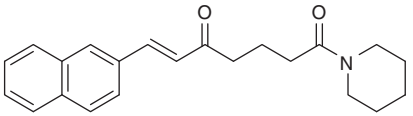	10 (34.00%)	>10	>10	10 (36.83%)	>10	>10	–
XVIII	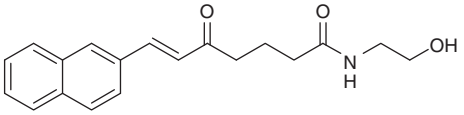	10 (4.58%)	>10	>10	10 (72.02%)	4.08	1.03	>9.71
XIX	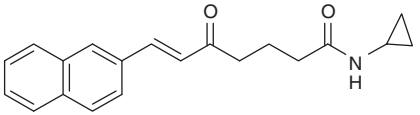	10 (15.28%)	>10	>10	10 (56.70%)	8.02	2.04	>4.90
XX	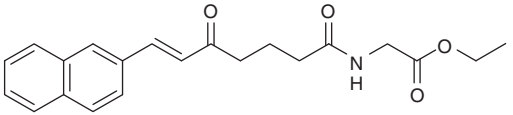	10 (41.55%)	>10	>10	10 (41.70%)	>10	>10	–
XXI	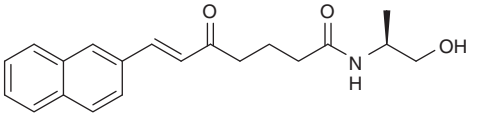	10 (0.00%)	>10	>10	10 (37.70%)	>10	>10	–
XXII	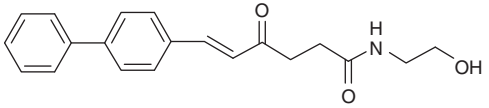	10 (5.25%)	>10	>10	10 (46.11%)	>10	>10	–
XXIII	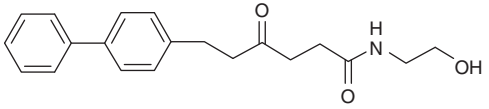	10 (10.89%)	>10	>10	10 (52.95%)	8.85	2.25	>4.44
XXIV	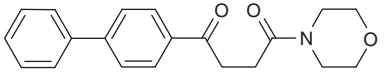	10 (12.22%)	>10	>10	10 (14.87%)	>10	>10	–

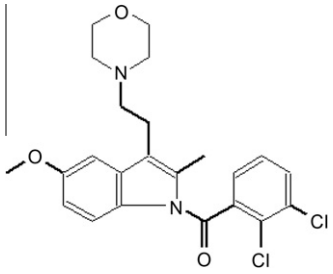

Figure 2. GW405833 a selective CB2 agonist.

Table 2.[22] The alignment shows consensus with that of CB1 to the β2 adrenergic receptor proposed by Shim et al. For construction of the helical bundle of the CB2 receptor, the helical boundaries, not TM boundaries, of the X-ray structure of β2AR were used to extract the secondary structural information as much as possible. The helical boundaries were assigned by STRIDE (Supplementary data, Figs. A-3 and A-4).[23] The template structure used in our study was crystallized in its inactive state[20,21,24,25], hence, CB2 receptor was activated according to the methods mentioned in the literature, to be able to dock the CB2 selective agonist GW405833 into it. The modeled activated structure of the GPCR receptor is determined by the different arrangement of TM3 and TM6. This hypothesis is based on the fact that the disruption of the interaction between these two helices produces constitutive modeled receptor activation. According to Ballesteros et al., the extent of the constitutive activation is closely correlated with the extent of conformational rearrangement in TM6.[26] Conformational switches in the TM helices can be generated as a result of the formation of the flexible molecular hinges by the residue Pro260 in CB2 in the highly conserved CWXP motif in TM6 (CWXP is CWFP in CB2 represented by Cys257, Trp258, Phe259 and Pro 260), Supplementary data, Figure A-5.[27]

During the modeled activation of β2-adrenergic receptor, Pro288 permits the movement of the intracellular end of TM6 away from TM3 and upwards towards the lipid bilayer, suggesting that the crucial movements for activation involve flexibility about the hinge formed by the highly conserved proline in TM6.[28] According to Shi et al. there is a rotamer toggle switch which is able to modulate the TM6 proline kink in the β2-adrenergic receptor and according to this hypothesis Cys285 trans/Trp286 gauche +/Phe290 gauche + represents the inactive form of the β2-adrenergic receptor while Cys285 gauche +/Trp286 trans/Phe290 trans represents the active state.[29] Concerning the CB receptor model activation, Singh and coworkers study showed that Trp258 and Phe117 interaction may act as toggle switch for CB2 activation with Trp258 gauche +/Phe117 trans representing the inactive form while Trp258 trans/Phe117 gauche + the CB2 active form.(Supplementary data, Fig. A-6).[30] Following these results, CB2 modeled activation was carried out by rotating TM3 and TM6 in counterclockwise direction (extracellular point of view) and TM6 was straightened using Pro260 as a flexible hinge. The suggested switch was finally toggled by adjusting the $\chi 1$ rotamer of Trp258 and Phe117 trans the former and gauche + the latter. This complies with Tuccinardi et al. regarding the CB1 activation.[17] The model of the TM helices was refined using minimization techniques (steepest descent and conjugate gradient) followed by 100 picosecond of molecular dynamics. No implicit solvent model was applied here; just a harmonic restraint was set on the backbone. The backbone conformation was evaluated using Psi/Phi Ramachandran plot. In addition Model verification was carried out using Modeler DOPE score and Verify 3D (Supplementary data, Fig. A-7).[31–33]

CB2 mutagenesis studies suggested the importance of Ser112[34] and Phe197[35] in this subtype. We choose the CB2 selective agonist GW405833 as a reference compound as it shares an aryl moiety at one end and an amine near the other end as in our compounds. We docked this ligand manually such that it complies with the above

Table 2
The secondary structure of β2 adrenergic receptor, CB1 receptor and CB2 receptor[a]

Helix	Start residue	Sequence	End residue
H1	30	2rh1 EVWVVGMGIVMSLIVLAIVFGNVLVITAIAK	60
	113	P21554 PSQQLAIAVLSLTLGTFTVLENLLVLCVILH	143
	30	P34972 GPQKTAVAVLCTLLGLLSALENVAVLYLILS	60
H2	67	2rh1 VTNYFITSLACADLVMGLAVVPFGAAHILM	96
	151	P21554 PSYHFIGSLAVADLLGSVIFVYSFIDFHVFI	180
	68	P34972 PSYLFIGSLAGADFLASVVFACSFVNFHVFI	97
H3	103	2rh1 NFWCEFWTSIDVLCVTASIETLCVIAVDRYFAIT	136
	186	P21554 RNVFLFKLGGVTASFTASVGSLFLTAIDRYISIH	219
	103	P34972 KAVFLLKIGSVTMTFTASVGSLLLTAIDRYLCLR	136
H4	147	2rh1 KNKARVIILMVWIVSGLTSFLPIQM	171
	230	P21554 RPKAVVAFCLMWTIAIVIAVLPLLG	254
	147	P34972 RGRALVTLGIMWVLSALVSYLPLMG	171
H5	197	2rh1 QAYAIASSIVSFYVPLVIMVFVYSRVFQEAKRQ	229
	272	P21554 DETYLMFWIGVTSVLLLFIVYAYMYILWKAHSH	304
	187	P34972 PNDYLLSWLLFIAFLFSGIIYTYGHVLWKAHQH	219
H6	266	2rh1 LKEHKALKTLGIIMGTFTLCWLPFFIVNIVHVI	298
	336	P21554 RMDIRLAKTLVLILVVLIICWGPLLAIMVYDVF	368
	238	P34972 RLDVRLAKTLGLVLAVLLICWFPVLALMAHSLA	270
H7	305	2rh1 KEVYILLNWIGYVNSGFNPLIYC	327
	376	P21554 KTVFAFCSMLCLLNSTVNPIIYA	398
	278	P34972 KKAFAFCSMLCLINSMVNPVIYA	300
H8	330	2rh1 PDFRIAFQELL	340
	402	P21554 KDLRHAFRSMF	412
	304	P34972 GEIRSSAHHCL	314

[a] The secondary structure of was assigned by Stride.[23] (2rh1) represents sequence of β2 adrenergic receptor, (P21554) represents the sequence of CB1 receptor and (P34972) represents the sequence of CB2 receptor. Conservancy of the aligned sequence by CLUSTALW (integrated in Discovery Studio)[23,42] is represented by (dark blue)for identical residues; (blue) for conserved substitutions and (light blue) for semi conserved substitutions. This alignment shows agreement with that done by shim regarding CB1.[43]

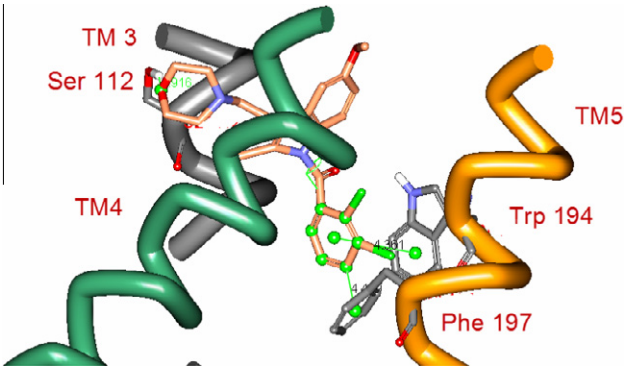

Figure 3. The CB2 selective agonist was manually docked such that its hydrophobic moiety (N^1-2,3dichlorobenzoyl) interacts with Phe197 and Trp94 while the morpholine group is positioned in a secondary lipophilic pocket. The main interactions proposed here are: the hydrogen bond with Ser112, the aromatic stacking of N^1-2,3-dichlorobenzoyl with Phe197 and the π–π interaction of N^1-2,3-dichlorobenzoyl with Trp194.

mentioned essential requirements, this was carried out by inserting the morpholinic group between TM3 and TM5, while the N^1-2,3-dichlorobenzoyl substituent was directed towards the central core of TM5 and TM6. This proposal complies with Tuccincardi et al.[17] In this manner the lipophilic core of the ligand was able to interact with Phe197 and the morpholinic core with Ser112, Figure 3. The complex was minimized using Steepest descent method and conjugate gradient with harmonic restraint on the backbone of the helix. Molecular dynamics (MD) simulation of the receptor–ligand complex was carried out to refine the model and test the stability of the proposed interactions of the ligand and the receptor during the production phase. Modeling the loops connecting the TM helices loops were added using Modeler,[33] where the modified helices were taken as reference template and β2 adrenergic receptor as the main template. Reference template co-ordinates were used as it is. EC2 was modeled according to Ahn et al.,[18] where the α-helix in the EC2 of β2-adrenergic receptor was introduced into CB2 maintaining the topological orientation observed for β-2 adrenergic receptor in the X-ray structure, Figure 4 and Supplementary data, Figure A-3. The minimization and MD protocol was carried out to refine the full receptor-complex using an implicit solvent model this time. The lipid bilayer was represented by the generalized Born solvent accessible surface area implicit membrane model of Spassov et al.[36] In this model, the aqueous solvent comprises a high dielectric region and the lipid membrane and the interior of the membrane bound protein taken together comprise a low dielectric region. The initial orientation of the GPCR agonist model with respect to the bilayer was refined via a rigid body procedure that systematically rotated and translated the complex to determine the optimal position of the complex relative to the implicit membrane. The membrane is presented as a planar low-dielectric slab and the molecule is treated as a rigid structure. The optimal orientation corresponds to the minimum of the solvation energy was calculated as in generalized Born solvent accessible surface area approximation. Minimization of the complex was carried out using GBIM. Molecular dynamics was carried out as a cascade of heating, equilibration and production to refine the complex and test the ligand stability in the proposed binding site. It is obvious that the essential interactions for the selective β2-agonist are as follows: hydrogen bond with Ser112, aromatic stacking of N^1-2,3-dichlorobenzoyl with Phe197 and π–π interaction of N^1-2,3-dichlorobenzoyl with Trp194, Figure 3. Field Align[15] was used to align the synthesized ligands to the bioactive conformer of the CB2 agonist GW405833. The idea behind this type of alignment is that two molecules which both bind to a common active site tend to make similar interactions with the protein and hence have highly similar field properties. Field alignment was used; taking into consideration the excluded volume provided by the binding site amino acid residues, to align the ligands to the bioactive conformer of the CB2 selective agonist, Figure 5. The main constraints which have been used were the field points representing the hydrophobic moiety and that representing the hydrogen bond acceptor.[37] The compounds which are top ranked in similarity index turned to have CB2 selectivity (see Table 3). Investigating the alignment of these compounds show high degree of compliance with the essential features which were constrained (hydrogen bond acceptor and hydrophobic aromatic feature. Investigating the compounds which have no CB2 activity reveals a high score of excluded volume clash penalty (compounds **X**, **XVII**, **XXI**, **XX** and **XV**) or in general they show no perfect mapping with the constrained field points (see Supplementary data, Fig. C1-20). In general the low similarity index scores are due to the design criteria which stress on two features only in the CB2 selective agonist (GW405833) and neglect any other feature.

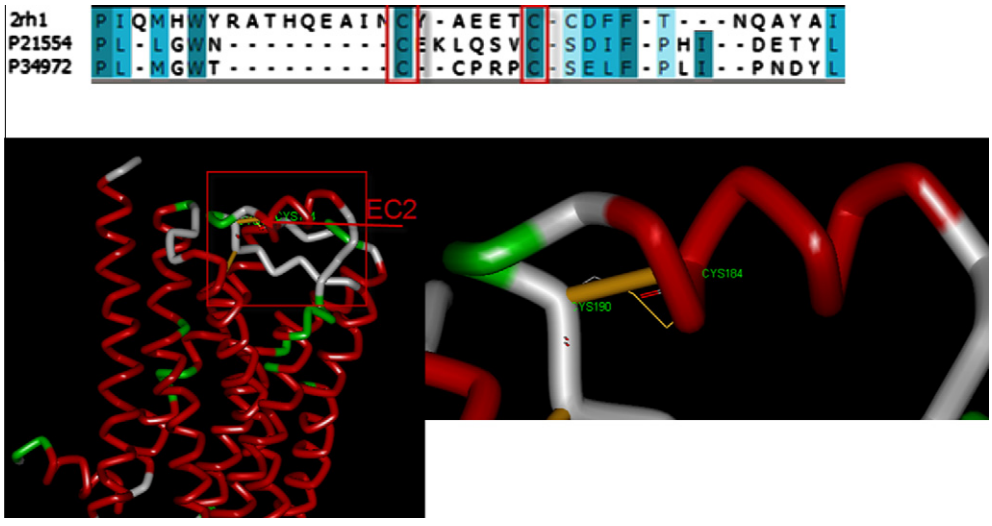

Figure 4. Sequence comparison of the EC2 loop. The residues which are involved in the disulfide bond of the EC2 loop are in red box. Shown here the sharing of the Cys-X-X-X-Ar motif among 2rh1 (β2-adrenergic receptor), P21554 (Cb1 receptor) and P34972 (Cb2 receptor).The motif in CB2 is represented by Cys179, Ser180, Glu181, Leu182 and Phe183. α-Helix in the EC2 of β2-adrenergic receptor is shown below with the disulfide bridge illustrated as yellow bridge.

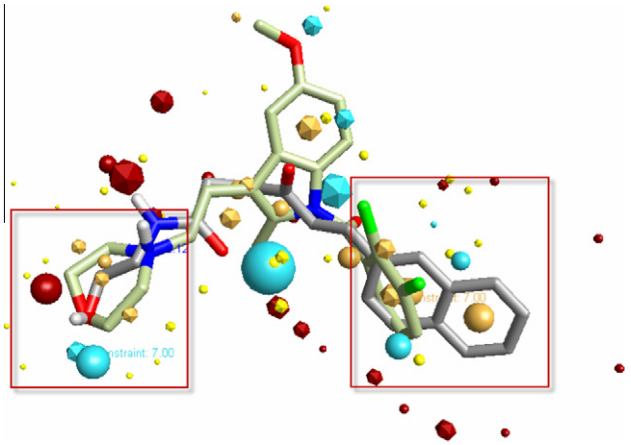

Figure 5. Ligand XI aligned to the CB2 selective agonist. Two constraints were applied. The first is the hydrophobic field point in the center of the N^1-2,3-dichlorobenzoyl (yellow sphere) and the second is the negative field point which represents H-bond donor on the protein (blue sphere). The field points interpretation is: Blue: Negative field points; Red: Positive field points; Yellow: van der Waals surface field points; Gold/Orange: Hydrophobic field points (describe regions with high polarisability/hydrophobicity).

Table 3
Field align similarity score of the newly synthesized ligands to that of the selective CB2 agonist (GW405833)[a]

Compd	Similarity	Compd	Similarity
XI	0.514	**XVI**	0.427
XVIII	0.512	**XV**	0.419
XIV	0.473	**XII**	0.414
XXIII	0.457	**XXII**	0.414
XIX	0.454	**XIII**	0.411
XXIV	0.449	**XX**	0.401
VIII	0.443	**VII**	0.364
IX	0.441	**III**	0.362
IV	0.439	**XVII**	0.355
XXI	0.433	**X**	0.322

[a] The top ranked ligands turned to have CB2 selectivity. In general, scores are low and we focus on two major essential features in GW405833 and neglect others.

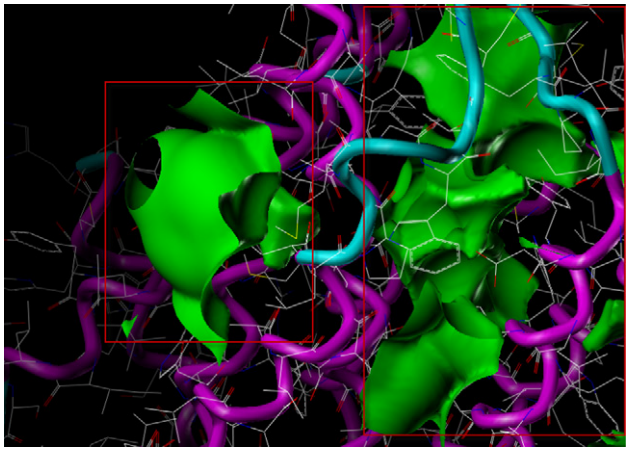

Figure 6. Grid analysis show comparative view of the large lipophilic pocket (right) to that of the small lipophilic pocket (left). Grid analysis was carried out using C1 = probe.

The MIF analysis was done to aid in explaining the SAR based on the nature of binding pocket. Binding site nature was investigated by Grid[39] software using different probes, Figure 6 and Supplementary data, Figure B-1. It reveals two binding pockets, large lipophilic pocket which encompass Phe197 and Trp194 and a small lipophilic pocket which encompass Ser112. This could explain the inactivity of ligands **III** and **IV** as they have a highly polarizable carboxylic group acting as hydrogen bond acceptor which is supposed to bind to Ser112 located in the small lipophilic pocket. Furthermore, this can explain the inactivity of ligands which have slightly polar groups attached to the hydrophobic moiety, for example, methoxy and dimethoxy derivatives of benzene if compared to naphthalene which is supposed to bind in the large lipophilic pocket.

SAR investigation and model support through docking the newly synthesized ligands was done using Gold[38] software, as it takes into consideration the features constraints as interaction filters. Compounds which have naphthalene moiety showed good activity due to the ideal interaction with Trp194 through π–π interaction together with the stacking interaction with Phe197, Figure 7.

Compounds **XI**, **XIV**, XVIII and **XIX** are good examples for this case. Only one compound with biaryl ring system showed activity (**XXIII**). The activity of this compound was low with respect to the naphthyl based ligands. Constrained docking gives some rational for this decrease in activity: The Torsion in case of biaryl system doesn't give the ideal orientation in space necessary for the interaction. The rotation about the single bond can form steric clash with Trp194 which can hinder the π–π interaction, Figure 8. The interaction can occur but with some torsional strain which give reason for the lowered activity. Pharmcophoric constraints showed some important aspects regarding the length of the side chain. It seems that there is an ideal distance between the centroid of the

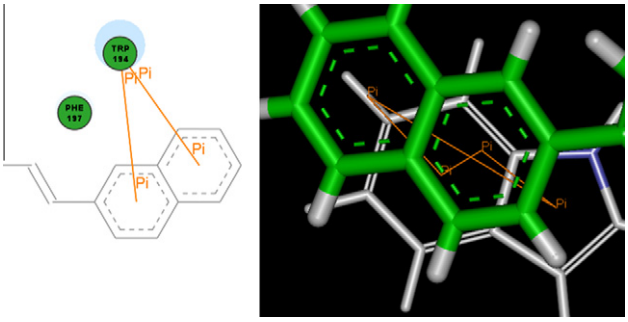

Figure 7. Naphthalene moiety is supposed to interact with Trp194 through π–π interaction. It seems that the hydrophobic interaction is strong in case of naphthalene being bicyclic like indole ring of tryptophan. Naphthalene interacts as well through stacking interaction with Phe197.

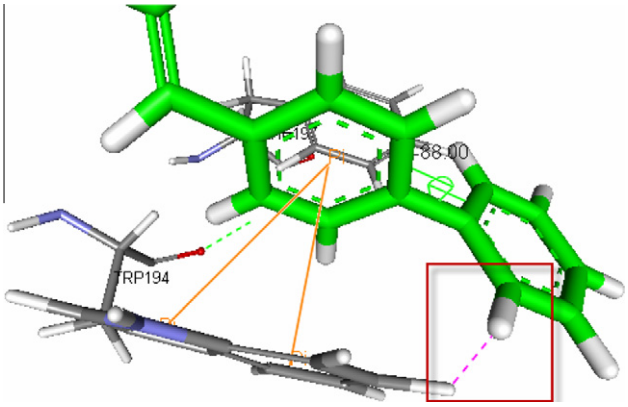

Figure 8. The biaryl system can form steric clash (shown in the red box) if it has to comply with the essential interaction with Trp194. This was shown through the constrained docking carried out by Gold. Otherwise some torsional strain is required to form the π–π interaction.

Table 4
Distance between the centroid of the hydrophobic aromatic feature and the hydrogen bond acceptor of the active compounds[a]

Drug	Distance
GW405833	9.808
XI	10.336
XVIII	11.264
XIX	9.903
XXIII	10.648
XIV	10.294

[a] Calculated from the manually docked CB2 selective ligand (GW 405833) and the automatically docked active ligands. The H-bond acceptor in **XI**, **XVIII** and **XXIII** is hydroxyl oxygen while in **XIX** and **XIV** is carbonyl oxygen.

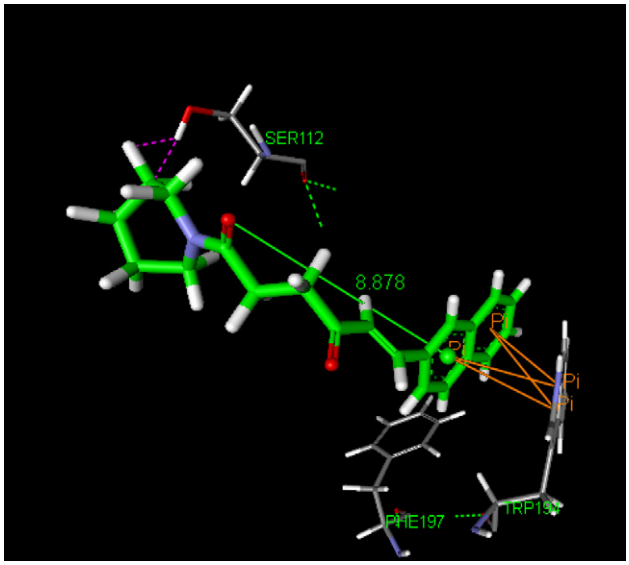

Figure 9. Compound **X** shows the absence of hydrogen bond interaction with serine 112 in the constrained docking run. The distance between the hydrophobic feature centroid and the hydrogen bond acceptor feature is 8.878 which is about 1 A less than desired range. Steric clash is shown (pink line). π–π interaction is shown in orange.

hyrdophobic aromatic feature and the hydrogen bond donor feature (Table 4). This distance ensures that the binding is ideal. Short distances will lead to failure in satisfaction of one of the essential interactions. Some compounds failed to attain this distance (**X**, **XIII** and **XXIV**), Figures 9–11.

It is proposed that hydrogen bond acceptor binds to Ser112 which is located in the small hydrophobic pocket. This hypothesis can be proved by testing the tolerance for different substituents which binds to this region. It is supposed that large substituents can make steric clash with the small lipophilic pocket residues. Docking studies and biological evaluation were used in this analysis. It is obvious from the docking study that bulky groups like phenyl (**IX**), piperidinyl (**X**, **XVII**) and diethanolamine (**XV**) are not tolerated. Constrained docking here is useful as it try to force the essential interactions, so any violations during this enforcement can be easily assessed by visual inspection, Figure 12, it is obvious that small head like cyclopropyl group is tolerated (**XIX**). It is important to mention though that (**XIII**) is not active though it has cyclopropyl group. This is mainly due to non compliance to the desired distance range mentioned before. Steric clash and the intolerance of the small lipophilic pocket explains the difference in activity between **XIV** and **XX**, see Figure 13. Docking showed that the bulky polar head has different roles in both compounds. In case of **XIV** the carbonyl group of the ethyl

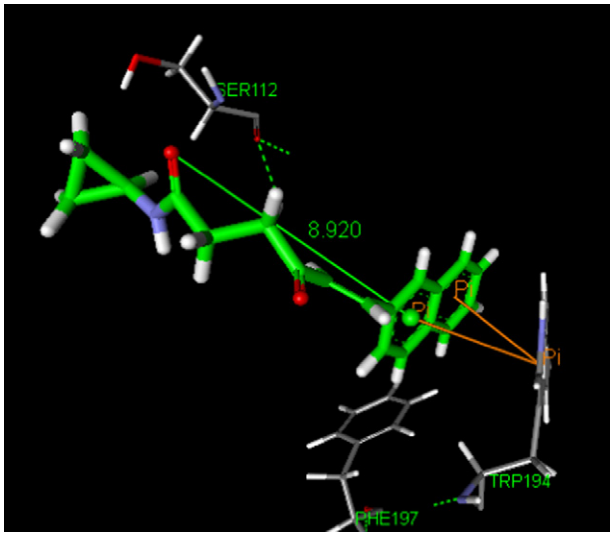

Figure 10. Compound **XIII** shows obvious non compliance with the desired distance range (the distance between the hydrophobic aromatic feature centroid and the hydrogen bond acceptor feature).

glycinate is the hydrogen bond acceptor and remaining part is small and can be easily accommodated. On the other hand **XX** forms hydrogen bond through the carbonyl group marked, Figure 13, leaving the whole ethyl glycinate in the lipophilic pocket which forms steric clash. Pharmacophore analysis using features instead of field points, showed results which are in consensus with the docking results, Figure 14. The compounds which fail to map completely were those lacking the essential distance between hydrophobic aromatic feature and hydrogen bond acceptor feature (**III**, **X**, **XIII** and **XXIV**) in addition to those which form steric clash in the small lipophilic pocket (**VII**, **XV** and **XVII**). Both **XXII** and **XXIII** showed very low fitting score (0.15, 0.52, respectively) this emphasis that the flexibility of **XXIII** gives it higher fit value. All compounds were also evaluated for their capability of inhibiting the enzymatic hydrolysis of radiolabelled anandamide by rat brain membranes, as the finding of such activity would represent indirect evidence for an amide to act as a potential substrate for FAAH. However, none of the amides exhibited any inhibitory activity up to a 50 μM concentration, thus ruling out the possibility of them being substrates for the enzyme and suggesting that they might be enzymatically stable at least as far as their metabolism by FAAH is concerned.

3. Conclusion

Our compounds represent a new class of CB2 selective ligands with the general formula: 6-(substituted-phenyl)-4-oxohex-5-enoic acid *N*-substituted amide and 6/7-naphthyl-4/5-oxohex-5-/hept-6-enoic acid *N*-substituted amide, to be reported for the first time. The molecular modeling study presented in this work provides a first study of CB2 in active form based on the structure of β2-adrenergic receptor. Furthermore, the model was designed complete with loops and helices and simulated using MD with implicit solvent membrane as a substitute to the resource intensive explicit models which use real phospholipid membranes. These combined approaches don't exist in one model for CB2 previously made in the literature. The constrained docking proved to be a valuable method to explain the SAR of the synthesized ligands. However for the purpose of screening, this model can be further validated using a library of actives and decoys to find the enrichment capability of the model. Based on the current study, we are

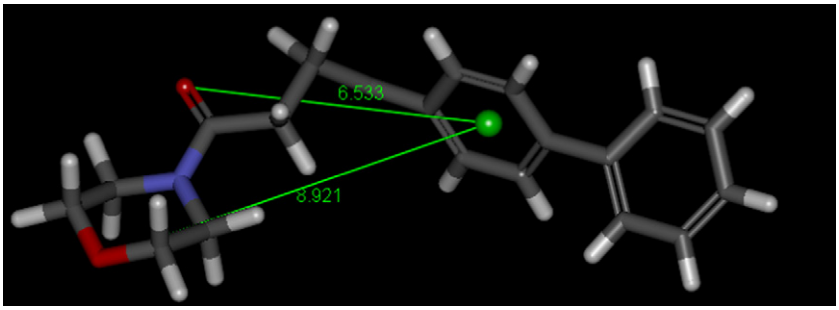

Figure 11. Compound **XXIV** shows noncompliance with the desired distance range (distance between hydrophobic aromatic feature and hydrogen bond acceptor feature).

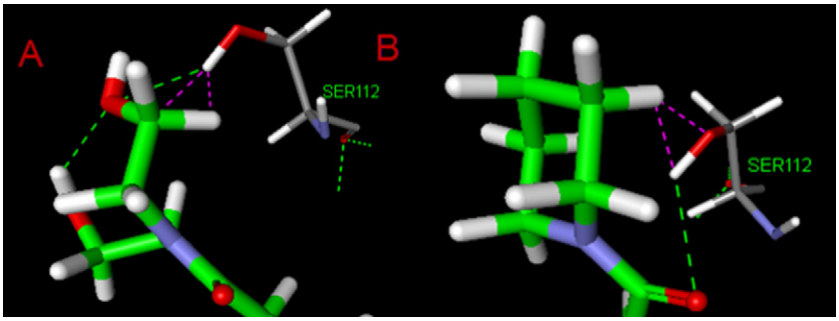

Figure 12. Diethanolamine in (**XV**) (A) and piperdinyl group in (**XVII**) (B) are not tolerated in the binding site. Constrained docking shows obvious steric clash with the small lipophilic binding site (shown here is Ser112 only) in order to achieve the essential H-bonding interaction with Ser112.

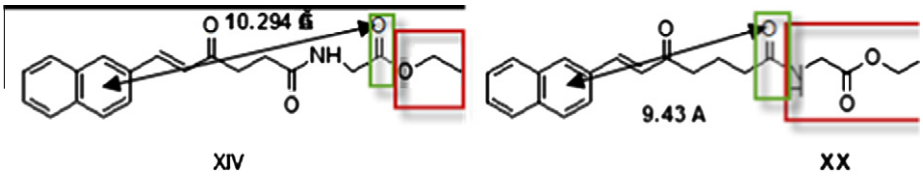

Figure 13. The compound **XX** inactivity is proposed to be due to the bulkiness of the head (shown in red box), although there is compliance with the distance range. The compliance of compound **XIV** with the desired distance range required between hydrophobic pocket and hydrogen bond acceptor together with the presence of small head which is tolerated in the small lipophilic pocket is the reason why **XIV** has activity

planning to further direct our research towards the design and synthesis of even more potent and selective compounds using the tailor-made homological model.

4. Experimental

4.1. Chemistry

All starting materials were obtained from Sigma–Aldrich and were used without further purification and all organic solvents used were obtained from Al-Goumhoria Company and were of general purpose grade. Melting points were determined on Buechi B-540 Melting Point apparatus and are uncorrected. FTIR spectra were recorded on Nicolet Avatar 380 spectrometer. ^{1}H NMR spectra were recorded on Varian Mercury VX-300 MHz spectrometer using $CDCl_3$ or DMSO-d_6 as a solvent; chemical shifts (δ) were reported in parts per million (ppm) downfield from TMS; multiplicities are abbreviated as: s: singlet; d: doublet; q: quartet; m: multiplet; dd: doublet of doublet; br: broad. Mass spectra were made on Hewlett–Packard GC–MS, model 5890, series II at an ionization potential of 70 eV. Elemental analyses were performed by the Microanalytical Unit, Faculty of Science, Cairo University; found values were within ±0.5% of the theoretical ones, unless otherwise indicated. Column chromatography was performed using silica gel 70–230 mesh. Reaction progress was monitored by TLC performed on pre-coated silica gel plates (ALUGRAM SIL G/UV254) and detection of the components was made by UV light (254 nm).

4.2. General procedure for the synthesis of (*E*)-6/7-(substituted-phenyl/naphthyl)-4/5-oxohex-5/hept-6-enoic acids (I–V)

Both the respective aldehyde (30 mmol) and levulinic acid (30 mmol) were dissolved in toluene (100 ml) containing acetic acid (3 ml) and piperidine (1 ml). The solution was heated under reflux using Dean-Stark water trap under nitrogen until the theoretical amount of water had been collected (~6 h) and TLC analysis ($CHCl_3$/CH_3OH, 93:7) indicated disappearance of the starting material. The solvent was evaporated in vacuo and after cooling the solid product was washed twice with 10 ml of diethyl ether and then twice with 15 ml of 2 M HCl, dried and recrystallized from the benzene.[13]

4.2.1. (*E*)-6-(3,4-Dimethoxyphenyl)-4-oxohex-5-enoic acid (I)[13]

Yellow crystals; yield: 62%; mp: 88–90 °C; ^{1}H NMR ($CDCl_3$): ^{1}H NMR ($CDCl_3$): 2.73 (t,, J = 6.6 Hz, 2H), 3.05 (t, J = 6.6 Hz, 2H), 3.92 (s, 6H), 6.68 (d, J = 15 Hz, 1H), 6.87 (d, J = 8.1 Hz, 1H), 7.12 (t, J = 9 Hz, 2H), 7.58 (d, J = 15 Hz, 1H); IR (cm^{-1}): 3150–2450 (–OH carboxylic

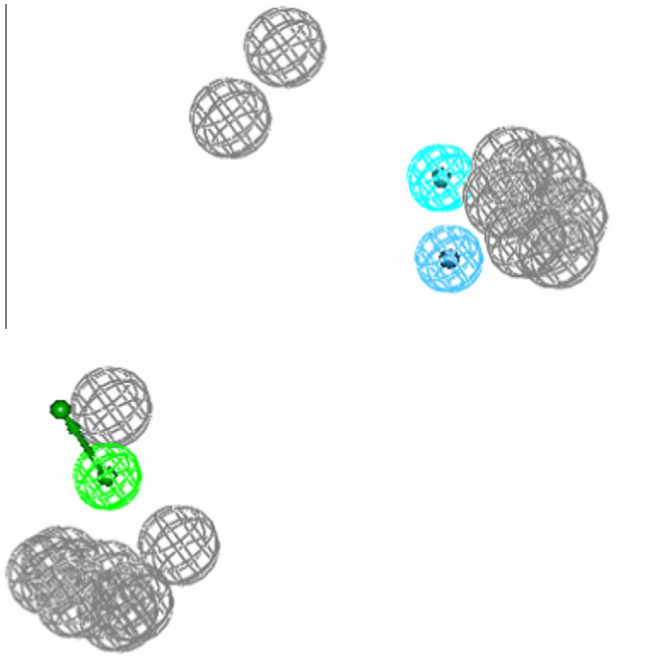

Figure 14. Pharmacophore manually created based on the bioactive conformer of GW405833, stressing on the hydrogen bond donor acceptor feature (green arrow), hydrophobe aromatic and hydrophobic point features. Excluded volume features were based on the amino acid residues of the binding site.

acid), 1721 (–C=O), 1674 (–C=O); MS (EI): *m*/*z* 264 (M^+), 64 (100%). Anal. Calcd for $C_{14}H_{16}O_5$ (m. wt. = 264.3): C, 63.63; H, 6.10. Found: C, 63.12; H, 5.80.

4.2.2. (*E*)-6-(4-Methoxyphenyl)-4-oxohex-5-enoic acid (II)[13]

Yellow crystals; yield: 60%, mp: 125–127 °C; ^{1}H NMR ($CDCl_3$): 2.75 (t, *J* = 6.6 Hz, 2H), 3.01 (t, *J* = 6.6 Hz, 2H), 3.89 (s, 3H), 6.66 (d, *J* = 15 Hz, 1H), 6.93 (d, *J* = 6.0 Hz, 2H), 7.49–7.53 (m, 2H), 7.58 (d, *J* = 15 Hz, 1H); IR (cm^{-1}): 3200–2500 (–OH carboxylic acid), 1718 (–C=O), 1672 (–C=O); MS (EI): *m*/*z* 235 (M^++1), 64 (100%). Anal. Calcd for $C_{13}H_{14}O_4$ (m. wt. = 234.2): C, 66.66; H, 6.02. Found: C, 66.21; H, 5.99.

4.2.3. (*E*)-6-Naphthalen-2-yl-4-oxohex-5-enoic acid (III)

Yellow crystals; yield: 67%; mp: 169–171 °C; ^{1}H NMR ($CDCl_3$): 2.79 (t, *J* = 6.6 Hz, 2H), 3.09 (t, *J* = 6.6 Hz, 2H), 6.90 (d, *J* = 15 Hz, 1H), 7.52–7.55 (m, 2H), 7.68–7.88 (m, 5H), 7.98 (s, 1H); IR (cm^{-1}): 3200–2400 (–OH carboxylic acid), 1688 (–C=O), 1679 (–C=O); MS (EI): *m*/*z* 254 (M^+), 181 (100%). Anal. Calcd for $C_{16}H_{14}O_3$ (m. wt. = 254.3): C, 75.57; H, 5.55. Found: C, 76.01; H, 5.51.

4.2.4. (*E*)-7-Naphthalen-2-yl-5-oxohept-6-enoic acid (IV)

Buff crystals; yield: 80%; mp: 172–174 °C; ^{1}H NMR ($CDCl_3$): 2.05–2.10 (m, 2H), 2.51 (t, *J* = 6.9 Hz, 2H), 2.84 (t, *J* = 6.9 Hz, 2H), 6.87 (d, *J* = 15 Hz, 1H), 7.52–7.55 (m, 2H), 7.68–7.87 (m, 5H), 7.98 (s, 1H); IR (cm^{-1}): 3200–2400 (–OH carboxylic acid), 1689 (–C=O), 1613 (–C=O); MS (EI): *m*/*z* 268 (M^+), 181 (100%). Anal. Calcd for $C_{17}H_{16}O_3$ (m. wt. = 268.3): C, 76.10; H, 6.01. Found: C, 76.10; H, 5.73.

4.2.5. (*E*)-6-Biphenyl-4-yl-4-oxohex-5-enoic acid (V)[13]

Yellow crystals; yield: 64%; mp: 188–190 °C; ^{1}H NMR ($CDCl_3$): 2.51 (t, *J* = 7.2 Hz, 2H), 2.95 (t, *J* = 7.2 Hz, 2H), 6.94 (d, *J* = 16.3 Hz, 1H), 7.35–7.50 (m, 3H), 7.67 (d, *J* = 16.3 Hz, 1H), 7.71–7.81 (m, 6H); IR (cm^{-1}): 3300–2400 (–OH carboxylic acid), 1713 (–C=O), 1684 (–C=O); MS (EI): *m*/*z* 280 (M^+), 77 (100%). Anal. Calcd for $C_{18}H_{16}O_3$ (m. wt. = 280.3): C, 77.12; H, 5.75. Found: C, 77.30; H, 5.79.

4.2.6. (*E*)-6-Biphenyl-4-yl-4-oxohexanoic acid (VI)

To a suspension of the (*E*)-6-biphenyl-4-yl-4-oxohex-5-enoic acid (**V**) (10.7 mmol) in methanol (50 ml), 300 mg of 10% Pd/C was added, the resultant mixture was hydrogenated at atmospheric pressure at room temperature for 2 h. The catalyst was filtered off, and the solvent was distilled in vacuum to obtain a white solid which was recrystallized from $CHCl_3$/hexane.[13]

4.2.7. (*E*)-6-Biphenyl-4-yl-4-oxohexanoic acid (VI)[13]

Fluffy white solid; yield: 70%; mp: 135–136 °C; ^{1}H NMR (DMSO-d_6): 2.40 (t, *J* = 7.5 Hz, 2H), 2.67 (t, *J* = 7.5 Hz, 2H), 2.80 (s, 4H), 7.26–7.60 (m, 9H), 12.0 (br s, 1H); IR (cm^{-1}): 3300–2400 (–OH carboxylic acid), 1718 (–C=O), 1704 (–C=O); MS (EI): *m*/*z* 282 (M^+), 167 (100%). Anal. Calcd for $C_{18}H_{18}O_3$ (m. wt. = 282.3): C, 76.57; H, 6.43. Found: C, 76.58; H, 6.41.

4.3. General procedure for the preparation of 6-(substituted-phenyl)-4-oxohex-5-enoic acid *N*-substituted amide (VII, VIII, IX, XXII, and XXIII)

A mixture of the appropriate acid (0.01 mol) and triethylamine (0.072 mol) in methylene chloride was cooled in an ice and salt bath to −10 °C. Ethyl chloroformate (0.05 mol) was added dropwise (while stirring) over a period of 10 min and stirring was continued for 30 min. The amine was added gradually within 10 min and stirring was continued overnight at room temperature. The solvent was then distilled under reduced pressure and the residue was extracted with ethyl acetate. The organic layer was then washed with saturated solutions of $NaHCO_3$, NH_4Cl, and H_2O (each three times with 50 ml, respectively) and dried over anhydrous $NaSO_4$. The solvent was evaporated under vacuum and the residue then washed finally with a mixture of diethyl ether/hexane or purified by column chromatography.[40]

4.4. General procedure for the preparation of 6/7-naphthyl-4/5-oxohex-5-/hept-6-enoic acid *N*-substituted amide (X–XXI)

A mixture of the appropriate acid (0.01 mol) and triethylamine (0.072 mol) in dry chloroform was cooled in an ice and salt bath to −10 °C. Tertiary butyl chloroformate (0.05 mol) was added dropwise (while stirring) over a period of 10 min and stirring was continued for 30 min. The amine was added gradually within 10 min and stirring was continued overnight at room temperature. The solvent was then distilled under reduced pressure and the residue was extracted with ethyl acetate. The organic layer was then washed with saturated solutions of $NaHCO_3$, NH_4Cl, and H_2O (each three times with 50 ml, respectively) and dried over anhydrous $NaSO_4$. The solvent was evaporated under vacuum and the residue then washed finally with a mixture of diethyl ether/*n*-hexane or purified by column chromatography.[40]

4.4.1. (*E*)-6-(3,4-Dimethoxyphenyl)4-oxohex-5-enoic acid piperedinamide (VII)

Dark brown crystals; yield: 35%; mp: 72–73 °C; ^{1}H NMR ($CDCl_3$): 1.57–1.66 (m, 6H), 2.73 (t, *J* = 6.9 Hz, 2H), 3.05 (t, *J* = 6.9 Hz, 2H), 3.51 (br s, 4H), 3.92 (s, 6H), 6.68 (d, *J* = 15 Hz, 1H), 6.87 (d, *J* = 8.1 Hz, 1H), 7.12 (t, *J* = 9 Hz, 2H), 7.58 (d, *J* = 15 Hz,1H); MS (EI): *m*/*z* 331 (M^+), 86 (100%). Anal. Calcd for $C_{19}H_{25}NO_4$ (m. wt. = 331.4): C, 68.86; H, 7.60, N, 4.23. Found: C, 69.31; H, 7.74; N, 4.45.

4.4.2. (*E*)-6-(3,4-Dimethoxyphenyl)-4-oxohex-5-enoic acid ethanolamide (VIII)

Brown powder; yield: 35%; mp: 83–85 °C; ^{1}H NMR ($CDCl_3$): 1.26 (t, J = 3.6 Hz, 2H), 2.58 (t, J = 6.6 Hz, 2H), 3.07 (t, J = 6.6 Hz, 2H), 3.72 (t, J = 4.5 Hz, 2H), 3.92 (s, 6H), 6.63 (d, J = 18 Hz, 1H), 6.87 (d, J = 8.1 Hz, 1H), 7.13 (t, J = 6 Hz, 2H), 7.55 (d, J = 18 Hz, 1H); IR (cm^{-1}): 3393 (–OH), 2929 (–CH aliphatic), 1641 (–C=O), 1632 (–C=O); MS (EI): m/z 307 (M^+), 191 (100%). Anal. Calcd for $C_{16}H_{21}NO_5$ (m. wt. = 307.3): C, 62.53; H, 6.89; N, 4.56. Found: C, 62.26; H, 6.95; N, 4.32.

4.4.3. (*E*)-*N*-(4-Hydroxyphenyl)-6-(4-methoxyphenyl)-4-oxohex-5-enamide (IX)

Dark brown powder; yield: 32%; mp: 125–127 °C; ^{1}H NMR ($CDCl_3$): 2.75 (t, J = 6 Hz, 2H), 3.19 (t, J = 6 Hz, 2H), 3.94 (s, 3H), 5.90 (br s, 1H, –NH), 6.66 (d, J = 18 Hz, 1H), 6.88 (d, J = 9 Hz, 4H), 7.13–7.16 (m, 4H, aromatic), 7.57 (d, J = 18 Hz, 1H); IR (cm^{-1}): 3319 (–OH), 3048 (–CH aromatic), 2921 (–CH aliphatic), 1658 (–C=O), 1650 (–C=O); MS (EI): m/z 325 (M^+), 59 (100%). Anal. Calcd for $C_{19}H_{19}NO_4$ (m. wt. = 325.4): C, 70.14; H, 5.89; N, 4.31. Found: C, 70.22; H, 5.83; N, 4.55.

4.4.4. (*E*)-6-Naphthalen-2-yl-4-oxohex-5-enoic acid piperidinamide (X)

Yellow powder; yield: 42%; mp: 110–112 °C; ^{1}H NMR ($CDCl_3$): 1.55–1.64 (m, 6H), 2.75 (t, J = 6 Hz, 2H), 3.10 (t, J = 6 Hz, 2H), 3.57 (br s, 4H), 6.92 (d, J = 15 Hz, 1H), 7.50–7.53 (m, 2H), 7.68–7.88 (m, 5H), 7.96 (s, 1H); IR (cm^{-1}): 3052 (–CH aromatic), 2923 (–CH aliphatic), 1683 (–C=O), 1635 (–C=O); MS (EI): m/z 321 (M^+), 84 (100%). Anal. Calcd for $C_{21}H_{23}NO_2$ (m. wt. = 321.4): C, 78.47; H, 7.21; N, 4.36. Found: C, 78.51; H, 7.42; N, 4.53.

4.4.5. (*E*)-6-Naphthalen-2-yl-4-oxohex-5-enoic acid ethanolamide (XI)

Yellowish-brown powder; yield: 45%; mp: 91–93 °C; ^{1}H NMR ($CDCl_3$): 2.61 (t, J = 7.5 Hz, 2H,), 3.14 (t, J = 6 Hz, 2H), 3.42–3.47 (m, 2H), 3.74 (t, J = 6 Hz, 2H), 6.30 (br s, 1H), 6.88 (d, J = 15 Hz, 1H), 7.48–7.55 (m, 2H), 7.67–7.86 (m, 5H), 7.97 (s, 1H); IR (cm^{-1}): 3252 (–OH), 3083 (–CH aromatic), 2918 (–CH aliphatic), 1684 (–C=O), 1653 (–C=O); MS (EI): m/z 297 (M^+), 151 (100%). Anal. Calcd for $C_{18}H_{19}NO_3$ (m. wt. = 297.4): C, 72.71; H, 6.44; N, 4.71. Found: C, 72.25; H, 6.28; N, 4.93.

4.4.6. (*E*)-6-Naphthalen-2-yl-4-oxohex-5-enoic acid (4-hydroxyphenyl)-amide (XII)

Dark brown powder; yield: 53%; mp: 131–133 °C; ^{1}H NMR ($CDCl_3$): 2.79 (t, J = 7.5 Hz, 2H), 3.20 (t, J = 7.5 Hz, 2H), 6.20 (br s, 1H), 6.66 (d, J = 18 Hz, 1H), 7.10–7.15 (m, 2H), 7.52–7.57 (m, 4H), 7.71–7.86 (m, 5H), 7.97 (s, 1H); IR (cm^{-1}): 3317 (–OH), 3060 (–CH aromatic), 2922 (–CH aliphatic), 1658 (–C=O), 1650 (–C=O); MS (EI): m/z 345 (M^++2), 237 (100%). Anal. Calcd for $C_{22}H_{19}NO_3$ (m. wt. = 345.4): C, 76.50; H, 5.54; N, 4.06. Found: C, 76.88; H, 5.62; N, 3.87.

4.4.7. (*E*)-6-Naphthalen-2-yl-4-oxohex-5-enoic acid cyclopropamide (XIII)

Red powder; yield: 45%; mp: 154–156 °C; ^{1}H NMR ($CDCl_3$): 0.52 (br s, 2H), 0.74–0.78 (m, 2H), 2.54 (t, J = 6.6 Hz, 2H), 2.71–2.73 (m, 1H), 3.11 (t, J = 6.6 Hz, 2H), 5.80 (br s, 1H), 6.88 (d, J = 15 Hz, 1H), 7.52–7.55 (m, 2H), 7.67–7.89 (m, 5H), 7.97 (s, 1H); IR (cm^{-1}): 3243 (–NH), 3051 (–CH aromatic), 2911 (–CH aliphatic), 1682 (–C=O), 1661 (–C=O); MS (EI): m/z 293 (M^+), 127 (100%). Anal. Calcd for $C_{19}H_{19}NO_2$ (m. wt. = 293.4): C, 77.79; H, 6.53; N, 4.77. Found: C, 77.50; H, 6.67; N, 4.81.

4.4.8. (*E*)-6-Naphthalen-2-yl-4-oxohex-5-enoic acid glycinamide ethyl ester (XIV)

Red powder; yield: 46%; mp: 92–95 °C; ^{1}H NMR ($CDCl_3$): 1.31 (t, J = 7.2 Hz, 3H), 2.67 (t, J = 6 Hz, 2H), 3.10 (t, J = 6 Hz, 2H), 4.03 (d, J = 8.4 Hz, 2H), 4.23 (q, J = 7.2 Hz, 2H), 6.31 (br s, 1H), 6.88 (d, J = 18 Hz, 1H), 7.51–7.54 (m, 2H), 7.67–7.86 (m, 5H), 7.96 (s, 1H); IR (cm^{-1}): 3308 (–NH), 3056 (–CH aromatic), 2980 (–CH aliphatic), 1737 (–CO), 1682 (–C=O), 1648 (–C=O); MS (EI): m/z 339 (M^+), 152 (100%). Anal. Calcd for $C_{20}H_{21}NO_4$ (m. wt. = 339.4): C, 70.78; H, 6.24; N, 4.13. Found: C, 70.39; H, 6.56; N, 4.20.

4.4.9. (*E*)-6-Naphthalen-2-yl-4-oxohex-5-enoic acid diethanolamide (XV)

Red solid; yield: 43%; mp: 94–96 °C; ^{1}H NMR ($CDCl_3$): 2.82 (t, J = 6 Hz, 2H), 3.15 (t, J = 6 Hz, 2H), 3.58–3.65 (m, 4H), 3.85–3.90 (m, 4H), 6.89 (d, J = 15 Hz, 1H), 7.50–7.54 (m, 2H), 7.66–7.88 (m, 5H), 7.96 (s, 1H); IR (cm^{-1}): 3307 (–OH), 3056 (–CH aromatic), 2929 (–CH aliphatic), 1660 (–C=O), 1651 (–C=O); MS (EI): m/z 341 (M^+), 74 (100%). Anal. Calcd for $C_{20}H_{23}NO_4$ (m. wt. = 341.4): C, 70.36; H, 6.79; N, 4.10. Found: C, 70.52; H, 6.77; N, 4.23.

4.4.10. (*E*)-6-Naphthalen-2-yl-4-oxohex-5-enoic acid (2-hydroxy-1(*R*)-methylethanolamide (XVI)

Red powder; yield: 66%; mp: 106–109 °C; ^{1}H NMR ($CDCl_3$): 1.20 (d, J = 6.9 Hz, 3H), 2.58 (t, J = 6.0 Hz, 2H), 3.09 (t, J = 9.0 Hz, 2H), 3.51–3.56 (m, 1H), 3.69 (d, J = 11 Hz, 2H), 4.06 (br s, 1H), 6.05 (br s, 1H), 6.87 (d, J = 15 Hz, 1H), 7.50–7.53 (m, 2H), 7.66–7.85 (m, 5H), 7.96 (s, 1H); IR (cm^{-1}): 3300 (–OH), 3056 (–CH aromatic), 2932 (–CH aliphatic), 1682 (–C=O), 1644 (–C=O); MS (EI): m/z 311 (M^+), 152 (100%). Anal. Calcd for $C_{19}H_{21}NO_3$ (m. wt. = 311.4): C, 73.29; H, 6.80; N, 4.50. Found: C, 73.51; H, 6.42; N, 4.29.

4.4.11. (*E*)-7-Naphthalen-2-yl-5-oxohept-6-enoic piperidinamide (XVII)

Yellow powder; yield: 55%; mp: 100–103 °C; ^{1}H NMR ($CDCl_3$): 1.57–1.59 (m, 6H), 2.04–2.08 (m, 2H), 2.48 (t, J = 7.2 Hz, 2H), 2.86 (t, J = 7.2 Hz, 2H), 3.52 (br s, 4H), 6.86 (d, J = 18 Hz, 1H), 7.51–7.54 (m, 2H), 7.73–7.87 (m, 5H), 7.97 (s, 1H); IR (cm^{-1}): 3061 (–CH aromatic), 2942 (–CH aliphatic), 1685 (–C=O), 1636 (–C=O); MS (EI): m/z 335 (M^+), 152 (100%). Anal. for $C_{22}H_{25}NO_2$ (m. wt. = 335.4): C, 78.77; H, 7.51; N, 4.18. Found: C, 79.15; H, 7.17; N, 4.33.

4.4.12. (*E*)-7-Naphthalen-2-yl-5-oxohept-6-enoic acid ethanolamide (XVIII)

Yellow crystals; yield: 48%; mp: 100–103 °C; ^{1}H NMR ($CDCl_3$): 2.01–2.11 (m, 2H), 2.31 (t, J = 7.5 Hz, 2H), 2.80 (t, J = 6.9 Hz, 2H), 3.41–3.46 (m, 3H), 3.73 (t, J = 5.1 Hz, 2H), 6.20 (br s, 1H), 6.84 (d, J = 18 Hz, 1H), 7.46–7.55 (m, 2H), 7.65–7.85 (m, 5H), 7.96 (s, 1H); IR (cm^{-1}): 3280 (–OH), 3057 (–CH aromatic), 2935 (–CH aliphatic), 1679 (–C=O), 1637 (–C=O); MS (EI): m/z 311 (M^+), 141 (100%). Anal. Calcd for $C_{19}H_{21}NO_3$ (m. wt. = 311.4): C, 73.29; H, 6.80; N, 4.50. Found: C, 72.85; H, 6.44; N, 4.89.

4.4.13. (*E*)-7-Naphthalen-2-yl-5-oxohept-6-enoic acid cyclopropylamide (XIX)

Buff powder; yield: 63%; mp: 125–126 °C; ^{1}H NMR ($CDCl_3$): 0.48–0.52 (m, 2H), 0.75–0.81 (m, 2H), 1.99–2.09 (m, 2H), 2.25 (t, J = 7.5 Hz, 2H), 2.74–2.86 (m, 3H), 5.78 (br s, 1H), 6.85 (d, J = 15 Hz, 1H), 7.50–7.56 (m, 2H), 7.67–7.89 (m, 5H), 7.97 (s, 1H); IR (cm^{-1}): 3235 (–NH), 3053 (–CH aromatic), 2968 (–CH aliphatic), 1682 (–C=O), 1661 (–C=O); MS (EI): m/z 307 (M^+), 152 (100%). Anal. Calcd for $C_{20}H_{21}NO_2$ (m. wt. = 307.4): C, 78.15; H, 6.89; N, 4.56. Found: C, 77.67; H, 6.48; N, 4.32.

4.4.14. (*E*)-7-Naphthalen-2-yl-5-oxo-hept-6-enoic acid glycinamide ethyl ester (XX)

Brown powder; yield: 40%; mp: 78–80 °C; ^{1}H NMR ($CDCl_3$): 1.29 (t, J = 7.2 Hz, 3H), 2.03–2.10 (m, 2H), 2.84 (t, J = 6.9 Hz, 2H), 3.11 (t, J = 7.2 Hz, 2H), 4.05 (d, J = 5.1 Hz, 2H), 4.21 (q, J = 7.2 Hz, 2H), 6.20 (br s, 1H), 6.86 (d, J = 15 Hz, 1H), 7.51–53 (m, 2H), 7.67–7.85 (m, 5H), 7.97 (s, 1H); IR (cm^{-1}): 3291 (–NH), 2943 (–CH aliphatic), 1739 (–CO), 1686 (–C═O), 1652 (–C═O); MS (EI): m/z 353 (M^+), 151 (100%). Anal. Calcd for $C_{21}H_{23}NO_4$ (m. wt. = 353.4): C, 71.37; H, 6.56; N, 3.96. Found: C, 71.74; H, 6.33; N, 4.28.

4.4.15. (*E*)-7-Naphthalen-2-yl-5-oxohept-6-enoic acid (2-hydroxy-1(*R*)-methylethanolamide (XXI)

Whitish-brown powder; yield: 65%; mp: 114–116 °C; ^{1}H NMR ($CDCl_3$): 1.19 (d, J = 6.9 Hz, 3H), 2.03–2.12 (m, 2H), 2.32 (t, J = 6.9 Hz, 2H), 2.82 (t, J = 6.6 Hz, 2H), 3.51–3.57 (m, 1H), 3.71 (d, J = 6 Hz, 2H), 4.11 (br s, 1H), 5.82 (br s, 1H), 6.86 (d, J = 18 Hz, 1H), 7.51–7.55 (m, 2H), 7.67–7.89 (m, 5H), 7.97 (s, 1H); IR (cm^{-1}): 3308 (–OH), 3056 (–CH aromatic), 2956 (–CH aliphatic), 1684 (–C═O), 1644 (–C═O); MS (EI): m/z 325 (M^+), 152 (100%). Anal. Calcd for $C_{20}H_{23}NO_3$ (m. wt. = 325.4): C, 73.82; H, 7.12; N, 4.30. Found: C, 74.25; H, 7.39; N, 4.64.

4.4.16. (*E*)-6-Biphenyl-4-yl-4-oxohex-5-enoic acid ethanolamide (XXII)

Dark brown solid; yield: 65%; mp: 77–79 °C; ^{1}H NMR ($CDCl_3$): 2.58 (t, J = 9 Hz, 2H), 3.11 (t, J = 6 Hz, 2H), 3.22–3.27 (m, 2H), 3.64 (t, J = 6 Hz, 2H), 6.30 (br s, 1H), 6.85 (d, J = 18 Hz, 1H), 7.26–7.96 (m, 10H); IR (cm^{-1}): 3254 (–OH), 3030 (–CH aromatic), 2923 (–CH aliphatic), 1656 (–C═O), 1554 (–C═O); MS (EI): m/z 325 (M^++2), 73 (100%). Anal. Calcd for $C_{20}H_{21}NO_3$ (m. wt. = 323.4): C, 74.28; H, 6.55; N, 4.33. Found: C, 73.86; H, 6.73; N, 4.75.

4.4.17. (*E*)-6-Biphenyl-4-yl-4-oxohexanoic acid ethanolamide (XXIII)

Dark brown crystals; yield: 45%; mp: 113–116 °C; ^{1}H NMR ($CDCl_3$): 2.4 (t, J = 7.5 Hz, 2H), 2.67 (t, J = 7.5 Hz, 2H), 2.80 (s, 4H), 3.22–3.27 (m, 2H), 3.64 (t, J = 6 Hz, 2H), 7.26–7.60 (m, 9H); IR (cm^{-1}): 3307 (–OH), 3063 (–CH aromatic), 2929 (–CH aliphatic), 1683 (–C═O), 1363 (–C═O); MS (EI): m/z 325 (M^+), 77 (100%). Anal. Calcd for $C_{20}H_{23}NO_3$ (m. wt. = 325.4): C, 73.82; H, 7.12; N, 4.30. Found: C, 73.89; H, 7.45; N, 4.69.

4.4.18. 1-Biphenyl-4-yl-4-morpholin-4-yl-butane-1,4-dione (XXIV)

The preparation of compound **XVIII** is made of a two-step reaction where the first step involves the conversion of fenbufen into its enol ester and the second step involves the conversion of the formed enol ester into its respective amide.

4.4.19. 5-Biphenyl-4-yl-3*H*-furan-2-one (fenbufen enol ester)[41]

To a boiling solution of fenbufen (2.54 g, 9.98 mmol) in dry toluene (40 ml), acetic acid anhydride was added dropwise until the entire solid was dissolved and a bright red homogenous liquid was obtained. The reaction was monitored by TLC. Quantitative conversion was observed after 6 h of heating. The reaction mixture was allowed to cool to room temperature and the product precipitated as glossy pink crystals. The resulting suspension was filtered. The solid was recrystallized from ethanol to yield 2.05 g (87%) of analytically pure material.

4.4.20. 1-Biphenyl-4-yl-4-morpholin-4-yl-butane-1,4-dione (XXIV)

To a solution of the fenbufen enol ester (450 mg, 1.90 mmol) in dry toluene (20 mL) morpholine (0.17 ml, 1.90 mmol) was added. The reaction mixture was stirred at room temperature and monitored by TLC. Quantitative conversion was observed after 4 h. The suspension was filtered and the residual solid crystallized from ethanol to yield 43% of a white powder.[41]

4.4.21. 1-Biphenyl-4-yl-4-morpholin-4-yl-butane-1,4-dione (XXIV)

White fluffy powder; yield: 43%; mp: 159–160 °C; ^{1}H NMR ($CDCl_3$): 2.81 (t, J = 6.6 Hz, 2H), 3.42 (t, J = 6.6 Hz, 2H), 3.63 (br s, 4H), 3.72 (br s, 4H), 7.40–7.51 (m, 3H), 7.62–7.72 (m, 4H), 8.10 (q, J = 4.8 Hz, 2H); IR (cm^{-1}): 3050 (–CH aromatic), 2958 (–CH aliphatic), 1679 (–C═O), 1652 (–C═O); MS (EI): m/z 323 (M^+), 152 (100%). Anal. Calcd for $C_{20}H_{21}NO_3$ (m. wt. = 323.4): C, 74.28; H, 6.55; N, 4.33. Found: C, 73.88; H, 6.72; N, 4.73.

Acknowledgment

The authors are grateful to the Faculty of Postgraduate Studies, German University in Cairo, for partial financing of this work

Supplementary data

Supplementary data associated with this article can be found, in the online version, at doi:10.1016/j.bmc.2010.10.050.

References and notes

1. Vemuri, V. K.; Janero, D. R.; Makriyannis *Physiol. Behav.* **2008**, *93*, 671.
2. Gaoni, Y.; Mechoulam, R. *J. Am. Chem. Soc.* **1964**, *86*, 1646.
3. Devane, W. A.; Dysarz, F. A.; Johnson, M. R.; Melvin, L. S.; Howlett, A. C. *Mol. Pharmacol.* **1988**, *34*, 605.
4. Matsuda, L. A.; Lolait, S. J.; Brownstein, M. J.; Young, A. C.; Bonner, T. I. *Nature* **1990**, *346*, 561.
5. Munro, S.; Thomas, K. L.; Abu-Shaar, M. *Nature* **1993**, *365*, 61.
6. Devane, W. A.; Hanus, L.; Breuer, A.; Pertwee, R. G.; Stevenson, L. A.; Griffin, G.; Gibson, D.; Mandelbaum, A.; Etinger, A.; Mechoulam, R. I. *Science* **1992**, *258*, 1946.
7. Mechoulam, R.; Ben-Shabat, S.; Hanus, L.; Ligumsky, M.; Kaminski, N. E.; Schatz, A. R.; Gopher, A.; Almog, S.; Martin, B. R.; Compton, D. R. *Biochem. Pharmacol.* **1995**, *50*, 83.
8. Sugiura, T.; Kondo, S.; Sukagawa, A.; Nakane, S.; Shinoda, A.; Itoh, K.; Yamashita, A.; Waku, K. *Biochem. Biophys. Res. Commun.* **1995**, *215*, 89.
9. Beltramo, M.; Stella, N.; Calignano, A.; Lin, S. Y.; Makriyannis, A.; Piomelli, D. *Science* **1997**, *277*, 1094.
10. Cravatt, B. F.; Giang, D. K.; Mayfield, S. P.; Boger, D. L.; Lerner, R. A.; Gilula, N. B. *Nature* **1996**, *384*, 83.
11. Dinh, T. P.; Carpenter, D.; Leslie, F. M.; Freund, T. F.; Katona, I.; Sensi, S. L.; Kathuria, S.; Piomelli, D. B. *Proc. Natl. Acad. Sci. U.S.A.* **2002**, *99*, 10819.
12. Pacher, P.; Batkai, S.; Kunos, G. *Pharmacol. Rev.* **2006**, *58*, 389.
13. Abouzid, K.; Frohberg, P.; Lehmann, J.; Decker, M. *J. Med. Chem.* **2007**, *3*, 433.
14. Gallant, M.; Dufresne, C.; Gareau, Y.; Guay, D.; Leblanc, Y.; Prasit, P.; Rochette, C.; Sawyer, N.; Slipetz, D. M., et al *Bioorg. Med. Chem. Lett.* **1996**, *6*, 2263.
15. Fieldalign 2.1 Cresset-BMD (http://www.cresset-bmd.com/product/fieldalign).
16. de Graaf, C.; Rognan, D. *Curr. Pharm. Des.* **2009**, *15*, 4026.
17. Tuccinardi, T.; Ferrarini, P. L.; Manera, C.; Ortore, G.; Saccomanni, G.; Martinelli, A. *J. Med. Chem.* **2006**, *49*, 984.
18. Ahn, K. H.; Bertalovitz, A. C.; Mierke, D. F.; Kendall, D. A. *Mol. Pharmacol.* **2009**, *76*, 833.
19. Diaz, P.; Phatak, S. S.; Xu, J.; Astruc-Diaz, F.; Cavasotto, C. N.; Naguib, M. *J. Med. Chem.* **2009**, *52*, 433.
20. Rosenbaum, D. M.; Cherezov, V.; Hanson, M. A.; Rasmussen, S. G. F.; Thian, F. S.; Kobilka, T. S.; Choi, H.-J.; Yao, X.-J.; Weis, W. I.; Stevens, R. C.; Kobilka, B. K.; Pierce, K. L.; Premont, R. T.; Lefkowitz, R. J.; Kobilka, B. K.; Deupi, X.; Cherezov, V.; Rasmussen, S. G. F. *Science* **2007**, *318*, 1266.
21. Cherezov, V.; Rosenbaum, D. M.; Hanson, M. A.; Rasmussen, S. G. F.; Thian, F. S.; Kobilka, T. S.; Choi, H.-J.; Kuhn, P.; Weis, W. I.; Kobilka, B. K.; Stevens, R. C.; Takeda, S.; Kadowaki, S.; Haga, T.; Takaesu, H.; Mitaku, S.; Fredriksson, R.; Lagerstrom, M. C.; Lundin, L. G.; Schioth, H. B.; Pierce, K. L.; Premont, R. T.; Lefkowitz, R. J.; Shenoy, S. K.; Rosenbaum, D. M. *Science* **2007**, *318*, 1258.
22. Mirzadegan, T.; Benko, G.; Filipek, S.; Palczewski, K. *Biochemistry* **2003**, *42*, 2759.
23. Frishman, D.; Argos, P. *Proteins* **1995**, *23*, 566.
24. Rasmussen, S. G. F.; Choi, H.-J.; Rosenbaum, D. M.; Kobilka, T. S.; Thian, F. S.; Edwards, P. C.; Burghammer, M.; Ratnala, V. R. P.; Sanishvili, R.; Fischetti, R. F.; Schertler, G. F. X.; Weis, W. I.; Kobilka, B. K. *Nature* **2007**, *450*, 383.
25. Kobilka, B.; Schertler, G. F. X. *Trends Pharmacol. Sci.* **2008**, *29*, 79.
26. Ballesteros, J. A.; Jensen, A. D.; Liapakis, G.; Rasmussen, S. G. F.; Shi, L.; Gether, U.; Javitch, J. A. *J. Biol. Chem.* **2001**, *276*, 29171.
27. Sansom, M. S. P.; Weinstein, H. *Trends Pharmacol. Sci.* **2000**, *21*, 445.

28. Jensen, A. D.; Guarnieri, F.; Rasmussen, S. G. F.; Asmar, F.; Ballesteros, J. A.; Gether, U. *J. Biol. Chem.* **2001**, *276*, 9279.
29. Shi, L.; Liapakis, G.; Xu, R.; Guarnieri, F.; Ballesteros, J. A.; Javitch, J. A. *J. Biol. Chem.* **2002**, *277*, 40989.
30. Singh, R.; Hurst, D. P.; Barnett-Norris, J.; Lynch, D. L.; Reggio, P. H.; Guarnieri, F. *J. Pept. Res.* **2002**, *60*, 357.
31. Fiser, A.; Do, R. K.; Sali, A. *Protein Sci.* **2000**, *9*, 1753.
32. Modeler 9v8 (http://www.salilab.org/modeller/).
33. Bowie, J. U.; Luthy, R.; Eisenberg, D. *Science* **1991**, *253*, 164.
34. Tao, Q.; McAllister, S. D.; Andreassi, J.; Nowell, K. W.; Cabral, G. A.; Hurst, D. P.; Bachtel, K.; Ekman, M. C.; Reggio, P. H.; Abood, M. E. *Mol. Pharmacol.* **1999**, *55*, 605.
35. Song, Z. H.; Slowey, C.-A.; Hurst, D. P.; Reggio, P. H. *Mol. Pharmacol.* **1999**, *56*, 834.
36. Spassov, V. Z.; Yan, L.; Szalma, S. I. *J. Phys. Chem.* **2002**, *106*, 8726.
37. Cheeseright, T.; Mackey, M.; Rose, S.; Vinter, A. *J. Chem. Inf. Model* **2006**, *46*, 665.
38. Gold v4.1 (http://www.ccdc.cam.ac.uk/products/gold_suite/).
39. Grid v22 Molecular Discovery Ltd (http://www.moldiscovery.com).
40. Ismail, M. A. H.; Lehmann, J.; Ella, D. A. A. E.; Albohy, A.; Abouzid, K. A. M. *Med. Chem. Res.* **2009**, *18*, 725.
41. Zohrabi-Kalantari, V.; Link, A. *Arch. Pharm. (Weinheim)* **2004**, *337*, 546.
42. Discovery studio 2.5.5 (http://accelrys.com/products/discovery-studio/).
43. Shim, J.-Y. *Biophys. J.* **2009**, *96*, 3251.